



Phosphorylation cascade regulates the formation and maturation of rotaviral replication factories

Jeanette M. Criglar^{a,1}, Ramakrishnan Anish^{b,1}, Liya Hu^b, Sue E. Crawford^a, Banumathi Sankaran^c, B. V. Venkataram Prasad^{a,b}, and Mary K. Estes^{a,d,2}

^aDepartment of Molecular Virology and Microbiology, Baylor College of Medicine, Houston, TX 77030; ^bVerna and Marrs McLean Department of Biochemistry and Molecular Biology, Baylor College of Medicine, Houston, TX 77030; ^cMolecular Biophysics and Integrated Bioimaging, Berkeley Center for Structural Biology, Lawrence Berkeley National Laboratory, Berkeley, CA 94720; and ^dDepartment of Medicine, Gastroenterology and Hepatology, Baylor College of Medicine, Houston, TX 77030

Contributed by Mary K. Estes, October 19, 2018 (sent for review October 13, 2017; reviewed by Oscar R. Burrone and Ulrich Desselberger)

The rotavirus (RV) genome is replicated and packaged into virus progeny in cytoplasmic inclusions called viroplasm, which require interactions between RV nonstructural proteins NSP2 and NSP5. How viroplasms form remains unknown. We previously found two forms of NSP2 in RV-infected cells: a cytoplasmically dispersed dNSP2, which interacts with hypophosphorylated NSP5; and a viroplasm-specific vNSP2, which interacts with hyperphosphorylated NSP5. Other studies report that CK1 α , a ubiquitous cellular kinase, hyperphosphorylates NSP5, but requires NSP2 for reasons that are unclear. Here we show that silencing CK1 α in cells before RV infection resulted in (i) >90% decrease in RV replication, (ii) disrupted vNSP2 and NSP5 interaction, (iii) dispersion of vNSP2 throughout the cytoplasm, and (iv) reduced vNSP2 protein levels. Together, these data indicate that CK1 α directly affects NSP2. Accordingly, an *in vitro* kinase assay showed that CK1 α phosphorylates serine 313 of NSP2 and triggers NSP2 octamers to form a lattice structure as demonstrated by crystallographic analysis. Additionally, a dual-specificity autokinase activity for NSP2 was identified and confirmed by mass spectrometry. Together, our studies show that phosphorylation of NSP2 involving CK1 α controls viroplasm assembly. Considering that CK1 α plays a role in the replication of other RNA viruses, similar phosphorylation-dependent mechanisms may exist for other virus pathogens that require cytoplasmic virus factories for replication.

virus factory | phosphorylation | viroplasm | NSP2 | CK1 α

Many viral pathogens, including both DNA viruses (poxviruses) and RNA viruses [rotavirus (RV), orthoreovirus, hepatitis C virus, dengue virus, Marburg virus] replicate in cytoplasmic compartments that are physical scaffolds composed of both viral and cellular proteins (1–3). These compartments, excluded from the rest of the cytoplasm, are sites where the virus genome is replicated and progeny particles are assembled. Such replication compartments are alternately known as virus factories, virus replication centers or complexes, and viroplasms. Exactly how these virus factories form is largely unknown, so it is intriguing to consider that there may be common mechanisms that initiate their formation and regulate their assembly.

RV-induced severe, dehydrating gastroenteritis remains a leading cause of morbidity and mortality in infants and children less than 5 y of age worldwide and accounts for greater than 200,000 deaths annually (4). To begin to understand the mechanism of replication factory assembly, we studied the assembly of RV replication complexes known as viroplasms. Viroplasm formation requires the interaction of two nonstructural proteins, NSP2 and NSP5, and expression of NSP2 with NSP5 in cells lacking all other viral proteins results in the formation of viroplasm-like structures (VLS) (5). Loss of either NSP2 or NSP5 abolishes viroplasm formation and rotavirus replication (6–9). While information about the individual characteristics of NSP2 and NSP5 and some knowledge of how they physically

interact are available, exactly how these two proteins initiate viroplasm formation remains unclear (10–12).

NSP2, a 35-kDa monomer, forms octamers in solution and has several enzymatic activities, including nucleoside-triphosphatase (NTPase), 5'-RNA triphosphatase (RTPase), and nucleoside-diphosphate (NDP) kinase-like activities (13–15). We previously reported the identification of two distinct forms of NSP2 that differ in temporal appearance and conformation in RV-infected cells (16). The first form of NSP2 appears ~2 h postinfection (hpi) and is observed dispersed (d) throughout the cytoplasm during the entire course of infection (dNSP2). In contrast, the second form of NSP2 appears ~3 hpi and is exclusively viroplasm localized (v) in discrete punctate structures with NSP5 (vNSP2). Based on its interactions with a specific monoclonal antibody, conformationally vNSP2 differs from dNSP2 at the C terminus and its defining epitope is sensitive to reducing agents. Additionally, vNSP2 is phosphorylated on serine 313 (S313) in the C terminus 40 times more often than dNSP2 (16). We predicted that the conformation of the C-terminal helical (CTH) tail region of vNSP2 may be required for interoctamer NSP2 interaction, such as in the “domain-swapping” model proposed

Significance

Many DNA and RNA virus pathogens replicate in cytoplasmic compartments composed of viral and cellular proteins called virus factories or viroplasms. Using rotavirus (RV) as a model, we found that RV nonstructural protein NSP2 has autokinase activity. The cellular kinase CK1 α additionally phosphorylates NSP2, triggering NSP2 octamers to form a lattice structure, and is required to build viroplasms. CK1 α and viroplasm-specific NSP2 (vNSP2) are essential for RV nonstructural protein NSP5 hyperphosphorylation and association with vNSP2 for viroplasm formation. Protein regulation by phosphorylation is a common biological mechanism, raising the possibility that similar phosphorylation-dependent virus factory assembly mechanisms exist for other viral pathogens.

Author contributions: J.M.C., R.A., L.H., S.E.C., B.V.V.P., and M.K.E. designed research; J.M.C., R.A., L.H., and B.S. performed research; B.S. contributed new reagents/analytic tools; J.M.C., R.A., L.H., S.E.C., B.V.V.P., and M.K.E. analyzed data; and J.M.C. and M.K.E. wrote the paper.

Reviewers: O.R.B., International Centre for Genetic Engineering and Biotechnology; and U.D., University of Cambridge.

Conflict of interest statement: Ulrich Desselberger and S.E.C. are coauthors on a 2016 review article, and Ulrich Desselberger, S.E.C., and M.K.E. are coauthors on a 2017 review article.

Published under the PNAS license.

Data deposition: The atomic coordinates and structure factors have been deposited in the Protein Data Bank, www.wwpdb.org (PDB ID codes 6AUK, 6CYA, and 6CY9).

¹J.M.C. and R.A. contributed equally to this work.

²To whom correspondence should be addressed. Email: mestes@bcm.edu.

This article contains supporting information online at www.pnas.org/lookup/suppl/doi:10.1073/pnas.1717944115/-DCSupplemental.

Published online December 3, 2018.

by Hu et al. (17), and might be the “trigger” for the formation of viroplasm, since loss of this region prevents the formation of VLS in cell culture (16).

NSP5 is an O-linked glycoprotein that is variably phosphorylated and migrates as multiple isoforms with differing molecular weights on SDS/PAGE gels. The 26- and 28-kDa isoforms are considered hypophosphorylated in contrast to the hyperphosphorylated isoforms that migrate significantly more slowly between 32 and 35 kDa (18–20). NSP5 plays a major role in viroplasm formation (9, 21). Interestingly, dNSP2 interacts with only hypophosphorylated NSP5, while vNSP2 interacts with only hyperphosphorylated NSP5, suggesting that both NSP2 and NSP5 must be phosphorylated to form viroplasm (16). Because no RV-encoded protein kinase has been described, we sought to identify cellular protein kinases that could phosphorylate NSP2. Casein kinase 1 alpha (CK1 α), a ubiquitous and constitutively active cellular kinase (22), is reported to play a role in viroplasm morphology via phosphorylation of NSP5 (23, 24). Phosphorylation of the NSP5 26-kDa isoform by CK1 α forms the 28-kDa isoform *in vitro*, and hyperphosphorylation of NSP5 to form the 32- to 35-kDa isoforms is reported to require NSP2 for unknown reasons (25).

Our studies found that viroplasm assembly and virus replication is dependent upon CK1 α phosphorylation of NSP2 at S313. Additionally, we discovered an autokinase activity for NSP2 that is associated with NSP2 conformational changes. We determined that CK1 α is not only required for the formation of hyperphosphorylated NSP5, as previously reported, but also for the phosphorylation of vNSP2, thus triggering its localization to sites of viroplasm formation, its association with hyperphosphorylated NSP5, and subsequent virus replication.

Results

CK1 α Is Required for Efficient Rotavirus Replication. Given the direct role CK1 α is reported to play in NSP5 phosphorylation and viroplasm morphology (24), we first examined CK1 α in RV-infected cells using immunofluorescence (IF) confocal microscopy. We observed increased expression of CK1 α in RV-infected cells compared with adjacent uninfected cells (Fig. 1A) and also confirmed colocalization of CK1 α with NSP2 and NSP5 in viroplasm as has been previously reported (Fig. 1B) (24). Silencing CK1 α using siRNA resulted in a >90% reduction in infectious virus

production, comparable to silencing NSP2 (Fig. 1C). This suggested that CK1 α has a more significant role in RV replication than was previously reported in which silencing CK1 α reduced infectivity by ~50% (24).

CK1 α Is Required for vNSP2 Association with NSP5 and Viroplasm Assembly. We next determined if silencing CK1 α affected the distribution of dNSP2 in the cytoplasm or the localization of vNSP2 into viroplasm. Using IF, we observed that silencing CK1 α had little effect on the dispersed pattern of dNSP2 compared with cells transfected with an irrelevant siRNA (Fig. 2A). Some areas of increased dNSP2 density were noted, as well as a decrease in signal from NSP5. In contrast, silencing CK1 α had a striking effect on vNSP2. Compared with the irrelevant siRNA control, vNSP2 exhibited an uncharacteristic dispersed-like phenotype, reminiscent of dNSP2, and also appeared in large, asymmetric structures that rarely colocalized with NSP5, as occurs in viroplasm (Fig. 2B). These results indicated that CK1 α is critical for viroplasm formation, specifically for characteristic vNSP2 assembly and its association with NSP5. This disruption in viroplasm assembly provides an explanation for why CK1 α is required for RV replication (Fig. 1C), and together these data support our hypothesis that viroplasm formation is phosphorylation dependent.

Silencing CK1 α Reduces vNSP2 and Prevents NSP5 Hyperphosphorylation.

Previous *in vitro* reports showed that NSP5 hyperphosphorylation is CK1 α and NSP2 dependent (23–25). In addition, we previously showed that interaction of dNSP2 and vNSP2 with NSP5 is dependent on NSP5 phosphorylation status. Specifically, dNSP2 interacts with only hypophosphorylated NSP5, and vNSP2 interacts with only hyperphosphorylated NSP5 (16). Therefore, we predicted that the lack of viroplasm formation and the apparent loss of interaction between vNSP2 and NSP5 in CK1 α -silenced cells was due to a loss of hyperphosphorylated NSP5. To evaluate the effect of CK1 α silencing on NSP2 and NSP5, we analyzed these proteins by Western blot (WB) in CK1 α siRNA-silenced and RV-infected cell lysates. One of the defining characteristics of NSP2 isolated from RV-infected cells is that vNSP2, unlike dNSP2, can be detected only in RV-infected cell lysates prepared and separated on SDS/PAGE gels under nonreducing conditions (16); therefore, all WBs to detect NSP2 in RV-infected cell lysate are performed under nonreducing

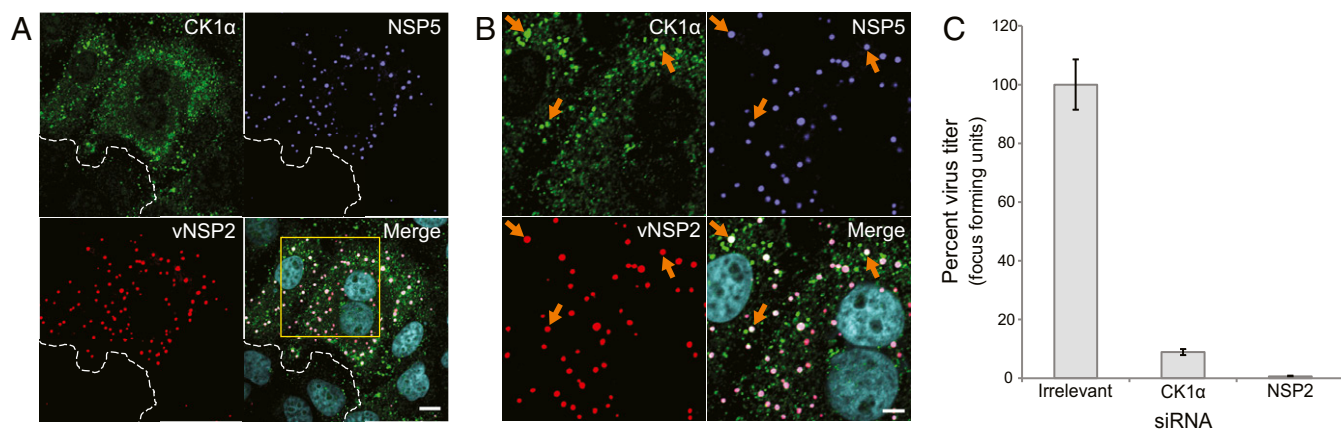


Fig. 1. CK1 α expression is required for RV replication. (A) Immunofluorescent detection of CK1 α (green) in RV-infected MA104 cells, 5 hpi, MOI 5. Viroplasm are detected using antibodies to vNSP2 (red) and NSP5 (purple). Cell nuclei are stained with DAPI (blue). Uninfected cells are delineated by a dotted white line. Images were obtained by confocal microscopy. (Scale bar: 10 μ m.) Images to verify that the secondary antibody used to detect CK1 α does not cross-react with the anti-vNSP2 or anti-NSP5 primary antibodies are shown in *SI Appendix*, Fig. S1. (B) Magnified view of the viroplasm-rich region (yellow box in A). Orange arrows show CK1 α , NSP2, and NSP5 proteins colocalizing in viroplasm. (Scale bar: 5 μ m.) (C) Effect of CK1 α silencing on RV replication. Virus was titered by fluorescent focus assay (FFA) and results are shown as percent virus titer compared with irrelevant siRNA control. The virus titer in CK1 α siRNA-transfected cells [5.0×10^4 focus-forming units (FFU)/mL] is compared with irrelevant siRNA-transfected (1.1×10^6 FFU/mL) and NSP2 siRNA-transfected (6.4×10^3 FFU/mL) cells. The assay was performed twice with three replicates. Error bars represent SD. Confirmation of CK1 α silencing by Western blot is shown in Fig. 2D, Lower panel.

NSP2. To determine if CK1 α phosphorylation was dependent on the enzymatic activity of NSP2, we constructed an NSP2 NTPase mutant, with the catalytic histidine at position 225 changed to alanine (NSP2 H225A), that is unable to hydrolyze ATP. The NSP2 H225A mutant was not able to autophosphorylate, but CK1 α phosphorylation was unimpaired (Fig. 3*A*, *Right*). This result confirmed that NSP2 auto-

phosphorylation is dependent on NSP2 NTPase activity and showed that CK1 α phosphorylation is independent of NSP2 enzymatic activity. When rNSP2 (*i*) without ATP, (*ii*) autophosphorylated, and (*iii*) CK1 α -phosphorylated were incubated with λ -phosphatase, the autoradiograph clearly shows the radiolabeled phosphates were removed (Fig. 3*B*).

NSP2 Autophosphorylation Is Consistent with Mass Spectrometry Analysis and Shows Dual-Specificity Autokinase Activity. Mass spectrometry analysis of autophosphorylated rNSP2 from the in vitro phosphorylation assay showed 22 phosphorylated amino acids with high confidence values (*SI Appendix*, Table S2). It is known that proteins exhibiting autokinase activity can autophosphorylate when expressed in bacteria (27), and indeed phosphorylation of NSP2 was detected in the bacterially expressed protein, as well as the NSP2 samples from the phosphorylation assay. Serines, threonines, and tyrosines were all phosphorylated, indicating that, at least in vitro, rNSP2 appears to have dual-specificity autokinase activity, acting as both a serine/threonine kinase as well as a tyrosine kinase. Mapping the autophosphorylated amino acids onto the NSP2 monomer shows that many of the identified phosphorylated residues are surface exposed and could be the result of *trans* autophosphorylation, particularly those that are located away from the NTPase active site, while others near the active site could result from *cis* autophosphorylation (Fig. 3*C*).

Crystal Structure of NSP2 Confirms the Protein Contains a Disulfide Bond. NSP2 contains four cysteine residues that are conserved among most group A rotaviruses. We have previously noted that NSP2 separated in nonreducing SDS/PAGE conditions is frequently observed as two or more distinct protein bands that differ in their rate of migration through the gel matrix. This is seen with NSP2 from RV-infected cell lysates (Fig. 2*C*) as well as with bacterially expressed rNSP2. We also discovered that addition of the γ [32 P]ATP radioisotope buffer alone to freshly purified rNSP2 catalyzes the formation of four NSP2 protein bands (*SI Appendix*, Fig. S3), demonstrating that NSP2 can be induced to form several intramolecular disulfide bridges. To determine if NSP2 forms disulfide bonds in RV-infected cells, we prevented the oxidation of free cysteines, which would result in the formation of additional disulfide bonds during the preparation of RV-infected cell lysates, with *N*-ethylmaleimide (NEM); this produced a single band of NSP2, demonstrating that NSP2 is an unstable and reactive protein that can form multiple disulfide linkages (*SI Appendix*, Fig. S4). However, because we previously predicted that NSP2 forms one disulfide bond, likely between Cys8 and Cys85 (16), we expressed NSP2 in Shuffle T7 *Escherichia coli* cells (Sh-NSP2) that are specifically designed to facilitate the formation of disulfide bonds in eukaryotic proteins that contain them. The resulting crystal structure of Sh-NSP2 (PDB ID code 6CY9) shows the formation of the predicted disulfide bridge between C8 and C85 (Fig. 4). The crystal structure shows that the side chain of C8 acquires an alternative conformation to form a disulfide bridge with C85. Determining whether disulfide-bonded NSP2 exists in the cell, or has a role in replication, is not known at this time.

CK1 α Phosphorylates NSP2 on Serine 313. Based on sequence alone, we initially predicted that S313 was the most likely target of CK1 α phosphorylation, as it resides in a canonical CK1 α consensus sequence, D/EXXS/T, where the n-3 residue is an acidic amino acid (28, 29). Mass spectrometry analysis of our phosphorylation assay samples showed several amino acids of rNSP2 were phosphorylated following incubation with CK1 α , but S313 was detected with low confidence and not reliable. To confirm S313 was phosphorylated by CK1 α , and also to determine if there were other CK1 α targets within NSP2, we constructed both an NSP2 S313A and an NSP2 S313D mutant. By

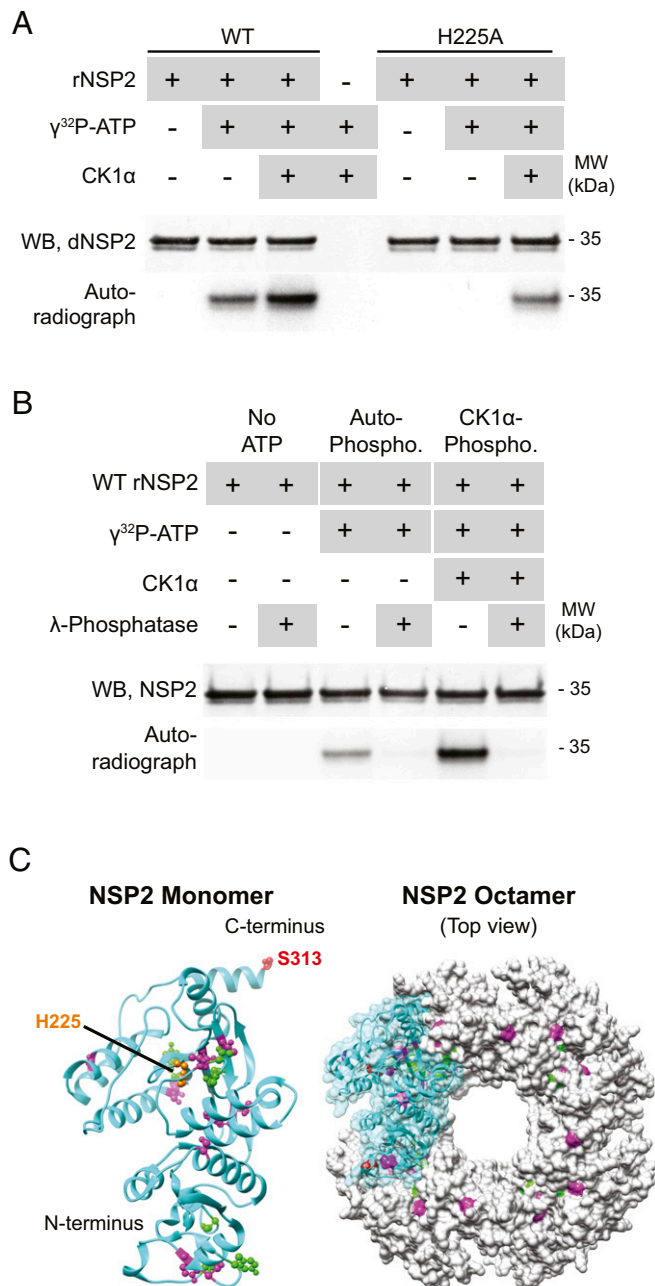


Fig. 3. NSP2 autophosphorylates and is phosphorylated by CK1 α . NSP2 was separated in reducing gels and detected by WB with anti-dNSP2 monoclonal antibody. Blots were exposed to autoradiography film overnight to detect the transfer of radiolabeled phosphate to NSP2. (A) Phosphorylation of WT (*Left*) and mutant H225A (*Right*) rNSP2 in the presence of γ [32 P]ATP and CK1 α . (B) Effect of lambda-phosphatase treatment on rNSP2, autophosphorylated rNSP2, and CK1 α -phosphorylated rNSP2. (C) Crystal structure of WT NSP2 monomer (cyan; PDB ID code 1L9V) and octamer, highlighting autophosphorylated residues (magenta), CK1 α -phosphorylated S313 (red), additional autophosphorylated residues detected after CK1 α -phosphorylation (green), and H225 (orange).

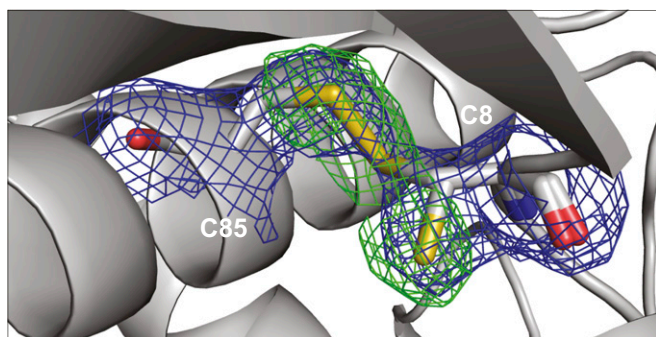


Fig. 4. NSP2 crystal structure shows a disulfide linkage between C8 and C85. Crystal structure of WT SA11 Sh-NSP2 (PDB ID code 6CY9) is shown. The simulated annealing $F_o - F_c$ difference electron density map (contoured at 3σ , green mesh) together with the $2F_o - F_c$ map (contoured at 1σ , blue mesh) clearly indicates that the side chain of C8 adopts a conformation that forms a disulfide bridge (yellow) with C85. The nitrogen (blue), oxygen (red), and sulfur (yellow) elements of C8 and C85 have been colored separately.

replacing S313 with alanine, we prevented CK1 α phosphorylation of S313 and could assess whether NSP2 was phosphorylated at other sites, and by replacing S313 with aspartic acid, we chemically mimicked a phosphorylated serine, allowing us to observe the effect of “phospho-NSP2” on the NSP2 structure (described below). To remove any contribution to phosphorylation by NTPase-dependent autophosphorylation, we constructed these mutants in a H225A background. No amino acids were phosphorylated by CK1 α in the S313 mutants, indicating that S313 is the target of CK1 α (Fig. 5). These experiments, however, cannot rule out that another amino acid already autophosphorylated by NSP2 could potentially be phosphorylated by CK1 α .

Crystal Structure of NSP2 S313D Shows Interoctamer Associations.

S313 resides within the C-terminal helix (CTH) domain of NSP2 that is predicted to form interoctamer chains through domain swapping with the CTH on neighboring NSP2 octamers (17). We wanted to assess the contribution, if any, that a phosphorylated S313 might provide to the formation of NSP2 octamer chains. Crystallization of the phosphomimetic NSP2 S313D was performed and yielded protein crystals within 1 h, in stark contrast to wild-type (WT) NSP2 that forms crystals over several days (30). The crystal structure of NSP2 S313D reveals that the side chain of D313 forms a hydrogen bond with R287 of the neighboring NSP2 octamer, thus strengthening the interoctameric interactions and readily promoting the crystal lattice formation in the crystals (Fig. 6A). Modeling phosphoserine at position 313 shows that the phosphate group can interact with the positively charged side chain of R287 by forming two hydrogen bonds, indicating that phosphorylation of S313 leads to additional octamer–octamer interactions (Fig. 6B). Mutation of serine 313 to alanine (PDB ID code 6CYA) abolishes these interactions (Fig. 6C). Together, these data strongly support an NSP2 phosphorylation-dependent mechanism for viroplasm formation.

Discussion

The aim of our studies was to determine a mechanism for phosphorylation-dependent virus factory formation with implications for a range of viral pathogens that replicate in cytoplasmic inclusions. Using RV viroplasms as a model virus factory, we found that viroplasm assembly requires phosphorylation of RV nonstructural protein NSP2, one of two requisite viroplasm-forming proteins, by the cellular protein kinase CK1 α . Phosphorylation of NSP2 by CK1 α is essential for the dispersed form of NSP2 (dNSP2) to traffic to sites of viroplasm formation,

likely cellular lipid droplets (31, 32), where dNSP2 converts into the viroplasm-associated form (vNSP2). We showed that CK1 α phosphorylates NSP2 on S313 at the C terminus and determined that phospho-S313 facilitates interoctameric interactions not achieved by unmodified S313; these interactions may greatly increase the kinetics of NSP2 lattice formation, triggering rapid macromolecular assembly of vNSP2 octamers into viroplasmic structures, as hypothesized by Hu et al. (17). Viroplasm formation also requires the interaction of NSP2 with NSP5. NSP5 is hyperphosphorylated in RV-infected cells and, in this work, we confirmed reports that CK1 α is required for NSP5 hyperphosphorylation (23, 24). Without CK1 α , vNSP2 is detected dispersed in the cytoplasm, and the few inclusions of vNSP2 that do form generally lack NSP5, thus resulting in a >90% reduction in infectious virus production. We attribute this greater reduction in titer, compared with earlier reports, to improved RNAi technology. These data show a phosphorylation-dependent mechanism for virus factory formation requiring a cellular protein kinase and coordinated phosphorylation of virus proteins that form these structures.

Previous *in vitro* studies showed that CK1 α -dependent hyperphosphorylation of NSP5 is NSP2 dependent. Our studies demonstrated it is likely vNSP2, and not dNSP2, that has a role in NSP5 hyperphosphorylation, since cells lacking CK1 α showed a marked decrease in vNSP2 formation. However, further studies are required to determine the role of vNSP2 in NSP5 hyperphosphorylation. Our current studies also revealed that during ATP hydrolysis, NSP2 not only transiently autophosphorylates the catalytic H225, but that this NTPase activity results in NSP2 autophosphorylation of several amino acids throughout the protein. This newly described autokinase activity for NSP2 suggests that NSP2 could phosphorylate other proteins, such as NSP5.

Mass spectroscopic analysis of rNSP2 from the autophosphorylation assay identified several phosphorylated serines/threonines and tyrosines, indicating that NSP2 has a previously unrecognized dual-specificity autokinase activity. These phosphorylated residues could be sites of *trans* and *cis* autophosphorylation that will require further investigation. While a number of phosphorylated serines and tyrosines were identified in our mass spectrometry analysis with high confidence, surprisingly phospho-S313 was not reliably detected (below the confidence level). However, we previously identified and confirmed by mass spectrometry phospho-S313 on NSP2 isolated from RV-infected cells, in particular vNSP2 (16), and this current manuscript provides further evidence using S313 mutants to confirm that the only residue phosphorylated by CK1 α is S313. These data show that although mass spectrometry is a powerful tool, the data should be experimentally validated, and in reverse, it is important to

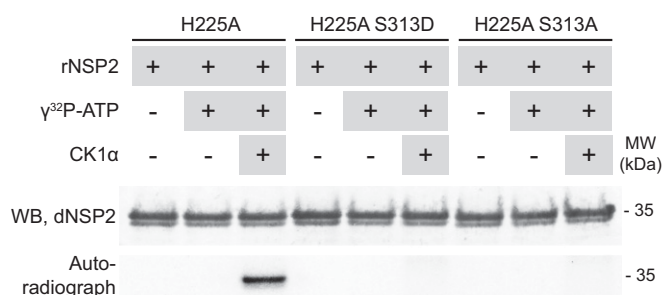


Fig. 5. CK1 α phosphorylates NSP2 on S313. NSP2 was detected in a reducing gel by WB with anti-dNSP2 monoclonal antibody. The blot was exposed to autoradiography film overnight to detect the transfer of radiolabeled phosphate to NSP2. CK1 α phosphorylation of NSP2 was determined using rNSP2 double mutants H225A S313D and H225A S313A. The autophosphorylation-deficient H225A single mutant, that is only phosphorylated by CK1 α , was used as a positive control.

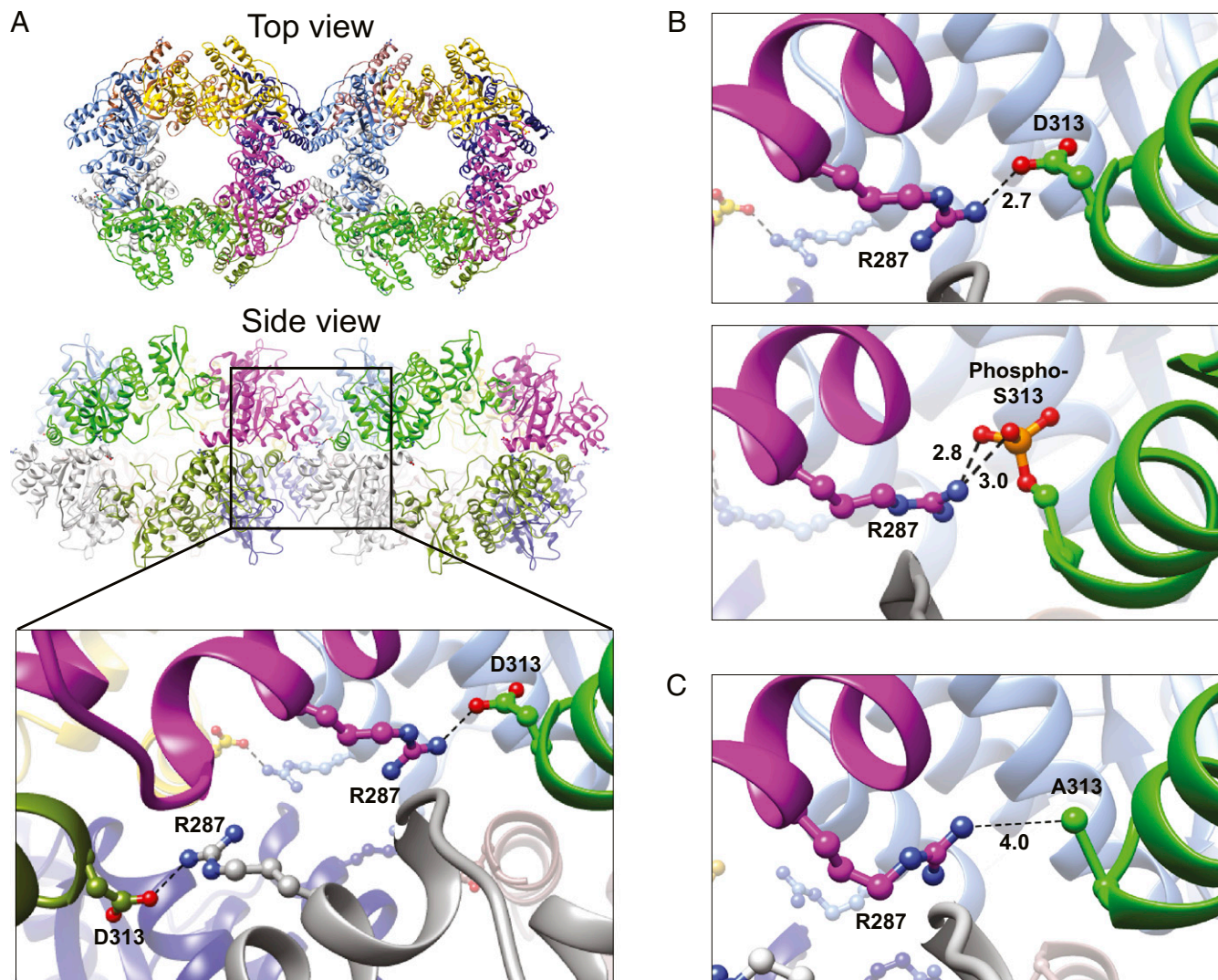


Fig. 6. Crystal structure of NSP2 S313D shows strong interoctamer hydrogen bond interactions. (A) Top and side views of the crystal structure of the NSP2 S313D phosphomimetic mutant (PDB ID code 6AUK) showing the interaction between two NSP2 octamers. Each NSP2 monomer is shown in a different color. The black box outlines the magnified view of the four interoctamer interactions formed between R287 and D313. (B) Serine phosphomimetic mutant S313D hydrogen bond interaction between D313 and R287 (2.7 Å) (Upper) compared with modeled phosphorylated S313 that can engage in two hydrogen bond interactions with R287 (3.0 Å and 2.8 Å) (Lower) demonstrating phosphorylated S313 can facilitate interoctamer interaction as observed in the crystal structure of NSP2 S313D. (C) Magnified view of NSP2 S313A crystal structure (PDB ID code 6CYA) showing A313 is positioned too distantly from R287 (4.0 Å) to form interoctamer interactions.

realize that residues not detected by mass spectrometry do not prove they do not exist. CK1 α , an S/T kinase, only phosphorylated NSP2 S313 in our assay and has never been reported to phosphorylate tyrosine; thus, it appears that the additional phosphorylated residues we detected in our CK1 α -treated samples are the result of further NSP2 autophosphorylation, triggered by CK1 α phosphorylation of S313. This is supported by the data (Fig. 5) showing no addition of ^{32}P to the S313A or S313D mutants in the presence of CK1 α . CK1 α phosphorylation of NSP2 S313 could induce conformational changes in the protein, exposing previously inaccessible residues for autophosphorylation. In addition, CK1 α phosphorylation is much more efficient if the target protein is already phosphorylated upstream of the target site (33). These coordinated, hierarchical phosphorylation events suggest a complex system of NSP2 regulation.

A proposed model illustrates the phosphorylation dependence for viroplasm assembly and includes a role for NSP2 as a protein kinase (Fig. 7). Our data support a model where nascent dNSP2 autophosphorylates at multiple sites via its NTPase activity and

associates with the 26-kDa hypophosphorylated NSP5. CK1 α phosphorylates dNSP2, while CK1 α and/or dNSP2 further phosphorylate NSP5 to the 28-kDa isoform. CK1 α phosphorylation triggers the dNSP2–NSP5 complex to traffic to sites of viroplasm formation. The mechanism by which CK1 α phosphorylation initiates the relocation of the NSP2–NSP5 complex is not yet known. It could be mediated by the association of NSP2 with new proteins via conformational changes following phosphorylation or the release of other proteins. Since viroplasms have been shown to form on lipid droplets (LDs) (32) conformational changes in NSP2, or NSP5, may expose lipophilic residues that allow the proteins to interact with cellular lipids bound for LDs. Several cellular proteins are inserted into LD membranes via amphipathic helices, e.g., perilipin (34). RV NSP5 possesses an amphipathic helix which theoretically could bind to LD membranes. Once at the site of viroplasm formation, vNSP2 protein lattice and domain swapping would induce the necessary curvature for viroplasm assembly. Concurrently, or rapidly following this

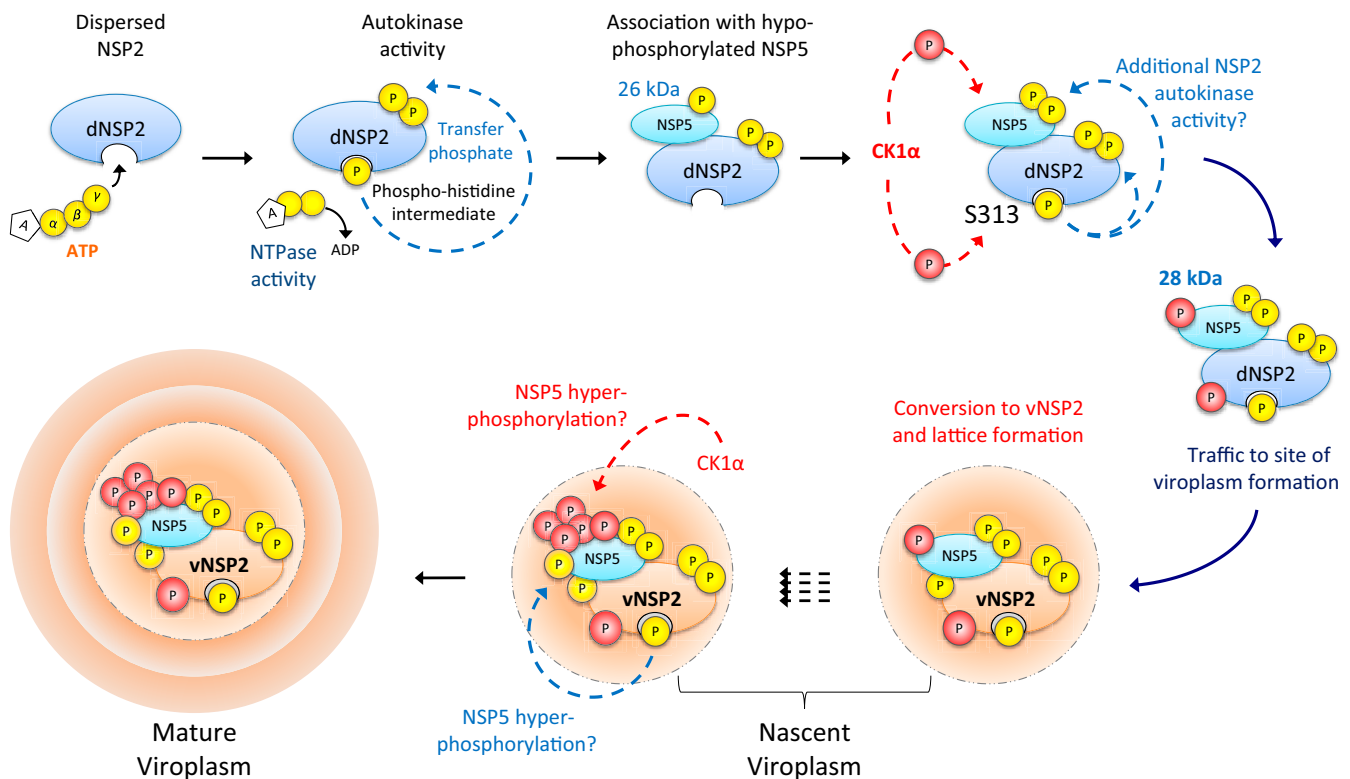


Fig. 7. Model of phosphorylation cascade and viroplasm assembly. Based on our studies we hypothesize that dNSP2 autophosphorylates via the NTPase activity, creating a transient phosphohistidine intermediate. Autophosphorylated NSP2 remains dispersed in the cytoplasm and associates with hypo-phosphorylated NSP5. CK1 α then phosphorylates NSP2 on S313. CK1 α may phosphorylate NSP5, leading to the appearance of the 28-kDa isoform. NSP2 may also phosphorylate NSP5. NSP2 phospho-S313 complexed with NSP5 traffics to the site of viroplasm formation and undergoes further conformational changes, by an unknown process, into vNSP2. NSP5 is rapidly hyperphosphorylated to the 32- to 35-kDa isoforms by CK1 α and/or NSP2 to remain associated with vNSP2. Repetition of this process leads to growth and maturation of the viroplasm.

event, NSP5 is hyperphosphorylated by CK1 α and/or NSP2, culminating in the growth of viroplasms, probably by the recruitment of other RV proteins by NSP2 and NSP5, both of which interact extensively with other viral proteins (12, 16, 21).

Protein kinases are often regulated by phosphorylation, which is a common biological mechanism to turn enzymes on and off. Phosphorylation can dramatically change the conformation of proteins, thus controlling access to catalytically active sites and regulating protein interactions by obscuring or revealing interacting domains, particularly with respect to kinases (35, 36). Phosphorylation of viral proteins is increasingly recognized as a regulator of RNA virus replication (37–39).

NSP2, both recombinant and WT NSP2 from RV-infected cell lysates, readily oxidizes to form several disulfide bond linkages if not prevented from doing so, but only the C8–C85 linkage was observed in the NSP2 crystal structure. Since NSP2 is a highly reactive protein in isolation, the formation of disulfide bridges must be tightly regulated or prevented in the cell. And if the C8–C85 linkage is biologically relevant, it would be an important aspect of RV replication to understand. We know that vNSP2 is conformationally distinct from dNSP2 and have shown that CK1 α phosphorylation of dNSP2 facilitates the change to vNSP2. However, it appears that CK1 α phosphorylation is not required for the conversion of dNSP2 into vNSP2, as this occurred to some degree in the absence of CK1 α . The dNSP2-to-vNSP2 conversion may be dependent on additional autophosphorylation or interaction with another RV protein, such as NSP5. Regardless, it is clear that the switch from dNSP2 to vNSP2 is a temporally controlled event during RV infection that

occurs only after CK1 α -phosphorylated dNSP2 traffics to, or assembles at, viroplasm assembly sites.

Phosphorylation has been shown to be important for protein–protein interactions, genome replication, and regulation of enzymatic activity. There are many recent examples of RNA virus replication that is regulated by protein phosphorylation and that specifically require CK1 α . Hepatitis C virus (HCV) NS5 protein is hyperphosphorylated by CK1 α during replication and causes localization of the protein to replication centers on lipid droplets (40–42). It is intriguing to speculate that, given our data, a similar mechanism may be used by RV to assemble NSP2 and NSP5 into viroplasms on lipid droplets. RNA replication of yellow fever virus is dependent on CK1 α phosphorylation of the methyltransferase on a residue conserved in all members of the flavivirus genus, including West Nile virus and dengue virus (43–47). Intriguingly, the RV methyltransferase, VP3, is predicted to be phosphorylated (48). CK1 α also phosphorylates the RNA-binding nucleocapsid of coronavirus avian infectious bronchitis virus. Phosphorylation of the nucleocapsid by CK1 α at the C terminus increases recognition and preferential binding of viral RNA substrates (49). Specific to RVs, we previously reported that mass spectrometry analysis of VP2 found in complex with vNSP2, but not dNSP2, is phosphorylated at S389 (16). Clearly, phosphorylation is a major regulator of viral replication. Therefore, autophosphorylation and CK1 α -mediated phosphorylation may also regulate other activities of NSP2, such as the NTPase, RTPase, RNA helicase, and ssRNA-binding activities during the replication cycle.

Taken together, our data suggest a phosphorylation-dependent mechanism for the formation of RV viroplasms. With the development of a reverse genetic system for RVs, these and other

observations can be systematically assessed in the RV system (50). Most intriguingly, however, our work suggests common mechanisms may exist for assembling the virus replication factories from other RNA viruses, one that utilizes a common cellular kinase, CK1 α , for localizing key components to sites of virus factory assembly. Cellular kinases are attractive targets for therapeutic intervention (38, 51). Agents designed to inhibit common targets, like cellular protein kinases, would allow the development of more broadly effective antivirals.

Materials and Methods

Virus, Cells, and Infections. Rotavirus strain SA11 4F G3P6[1] (52) was used to infect African green monkey kidney epithelial cells (MA104). MA104 cells were cultured and maintained in DMEM (Sigma) supplemented with 10% FBS (Corning) at 37 °C and 5% CO₂. Before infection, MA104 cells were either incubated overnight in DMEM without FBS or washed three times with PBS just before inoculation. SA11 4F was activated for 30 min in 10 μ g/mL trypsin (Worthington) in DMEM without FBS, and cells were inoculated with trypsin-activated virus, multiplicity of infection (MOI) 3 or 10, for 1 h at 37 °C, 5% CO₂. The inoculum was removed and replaced with DMEM without FBS or trypsin and incubated for an additional 4 or 5 h.

Virus Titration by Fluorescent Focus Assay. Methanol-fixed RV-infected cell monolayers were incubated with rabbit anti-RV primary polyclonal antibody serum (1:1,500 in PBS) for 2 h at 37 °C. Plates were washed three times with PBS and incubated with donkey anti-rabbit secondary antibody conjugated to fluorophore 488 (1:1,000 in PBS; Sigma) for 2 h at 37 °C. Plates were washed two times with PBS. Fluorescent foci were counted and fluorescent foci per milliliter sample were calculated.

SDS/PAGE Separation of RV Proteins. RV-infected cell lysates were prepared in nonreducing or reducing sample buffer (as needed to detect the different forms of NSP2 with monoclonal antibodies) (16) containing β -mercaptoethanol as indicated, and separated as previously described (16) using Criterion TGX 4–20% Precast Midi Protein Gels (Bio-Rad) in 1 \times Tris/glycine/SDS running buffer (Bio-Rad) (Fig. 2 C and D). Recombinant NSP2 proteins were separated by SDS/PAGE using Bolt 4–12% Bis-Tris Plus Gels (Thermo Fisher Scientific) in 1 \times Mes SDS Running Buffer (Thermo Fisher Scientific) using a Bolt Mini Gel Tank (Thermo Fisher Scientific) in nonreducing (*SI Appendix, Figs. S3 and S4*) or reducing (Figs. 3 A and B and 5) conditions. The lysates used for *SI Appendix, Fig. S4* were prepared as above with the addition of 20 mM NEM to control for artifactual disulfide bond formation.

Western Blot. Western blots were performed, as previously described (16). Primary monoclonal antibody supernatants to dNSP2 and vNSP2 (1:1,000), polyclonal guinea pig anti-NSP5 (1:1,000), have been previously described (16). RV antibodies and commercially available polyclonal immunogen-purified rabbit anti-CK1 α antibodies (1:200; Abcam), and mouse anti-tubulin (1:1,500; Sigma) were diluted in a 20% solution of SuperBlock (TBS) Blocking Buffer (Thermo Fisher Scientific). Secondary antibodies goat anti-mouse, goat anti-guinea pig, and goat anti-rabbit conjugated to alkaline phosphatase (1:3,000; Sigma) were diluted in 20% SuperBlock. Blots were washed once in TBS 0.1% Tween-20, and twice in TBS, before developing with a nitro-blue tetrazolium and 5-bromo-4-chloro-3'-indolylphosphate substrate reagent.

Immunofluorescence and Confocal Microscopy. IF confocal imaging was performed as previously described (16).

Primary antibodies. Mouse monoclonal antibody supernatants to dNSP2 and vNSP2 were used at 1:5, and polyclonal guinea pig anti-NSP5 serum (1203-3) was used 1:500. Polyclonal, immunogen affinity-purified, goat anti-CK1 α antibodies (Santa Cruz Biotechnology) were used at 1:50 as recommended by the manufacturer.

Secondary antibodies. Fig. 1: Donkey anti-goat-488, donkey anti-mouse-568, and donkey anti-guinea pig-633 (Alexa Fluor, Invitrogen Life Technologies) antibodies were used 1:1,000. Fig. 2: goat anti-mouse-488 and goat anti-guinea pig-568 (Alexa Fluor, Invitrogen Life Technologies) antibodies were used 1:1,000. All commercially available primary and secondary antibodies were confirmed to be free of rotavirus antibodies by WB and/or IF (*SI Appendix, Fig. S1*). DAPI was used to stain cell nuclei.

RNAi Assays. Subconfluent MA104 cells in six-well plastic culture dishes, or on glass coverslips, were transfected with a siRNA oligo pool specifically targeting CK1 α mRNA (Santa Cruz Biotechnology) using Lipofectamine

RNAiMAX transfection reagent per manufacturer's instructions (Invitrogen, Thermo Fisher Scientific). Cells were incubated for 48–72 h post-transfection (hpt). Before infection, the medium was removed, and the transfected cell monolayers were incubated in DMEM without serum 4–24 h before infection. Cells were infected with SA11 4F, MOI 3, as described above, and incubated for 6 h. Assays were performed twice, in triplicate.

Expression and Purification of rNSP2. Rotavirus SA11 (group A) NSP2 (GenBank accession no. Q03242) and the single (H225A and S313A) and double (H225A–S313A and H225A–S313D) mutants were cloned into pQE60 (Qiagen), a bacterial expression vector, with a C-terminal 6-His tag preceded by a thrombin cleavage site (LVPRGS), as described by Viskovska et al. (12). WT NSP2 and the mutant proteins were expressed in *E. coli* SG13009 cells and purified using affinity chromatography [Ni-nitrilotriacetic acid (Ni-NTA); Qiagen], followed by gel filtration chromatography (HiLoad 16/60 Superdex 200, GE Healthcare). Gel filtration profile confirmed that WT NSP2 and all of the mutants form an octamer in solution. Purified NSP2 was dialyzed into a final buffer containing 10 mM Tris-HCl (pH 7.8) and 100 mM NaCl. They were concentrated to 2 mg/mL using Amicon concentrators with a cutoff of 100 kDa and used for the phosphorylation assays. The NSP2 single mutant S313D of rotavirus strain SA11 was expressed and purified as previously described (17). WT disulfide-bonded NSP2 (Sh-NSP2) was expressed in Shuffle T7 *E. coli* cells (New England Biolabs) that are suitable for T7 protein expression with enhanced capacity to correctly fold proteins with multiple disulfide bonds in the cytoplasm and purified as above (12).

In Vitro Phosphorylation Assays. Purified rNSP2 proteins (2 mg/mL) were added to kinase reaction buffer on ice. Kinase reaction buffer final concentrations were as follows: PBS (0.01 M Na phosphate, 0.15 M NaCl), 1 \times Protein Kinase Buffer (50 mM Tris-HCl, 10 mM MgCl₂, 0.1 mM EDTA, 2 mM DTT, 0.01% Brij 35, pH 7.5; New England Biolabs), human CK1 α 1 enzyme (0.1 μ g/ μ L; Sigma), ATP cold (5 mM in H₂O; Invitrogen, Thermo Fisher Scientific), with or without γ [³²P]ATP (EasyTide 3K mCi/mL; Perkin-Elmer) or CK1 α and incubated for 2 h at 30 °C. Note: Perkin-Elmer isotopes contain proprietary buffers and stabilizing agents and were observed to enhance the formation of disulfide bonds in our phosphorylation assays (*SI Appendix, Fig. S3*). Additional studies to understand the nature of the disulfide bonds were carried out to define the contribution of each to NSP2 activity.

For lambda (λ)-phosphatase treatment, aliquots were removed from each sample, 400 units of λ -phosphatase were added (New England Biolabs), and the samples incubated at 30 °C for 2 h. All reactions were stopped by addition of SDS/PAGE Laemmli Sample Buffer (Bio-Rad) with β -mercaptoethanol or no reducing agent (*SI Appendix, Figs. S3 and S4*) and incubated for 10 min at 70 °C. Samples were loaded onto SDS/PAGE gels for separation and WB detection. Following separation, the proteins were transferred to nitrocellulose membranes, air dried, and exposed to autoradiography film overnight.

Crystallization of NSP2 S313D and S313A Mutants and Sh-NSP2. The purified NSP2 S313D was concentrated to 6 mg/mL in buffer containing 10 mM Tris, pH 8.0, 50 mM NaCl, and 1 mM DTT. The purified NSP2 S313A and Sh-NSP2 were concentrated to 5 mg/mL in a buffer containing 10 mM Tris, pH 8.0, 100 mM NaCl. The purified S313D protein was crystallized by hanging-drop vapor diffusion by mixing 0.2 μ L of protein with 0.2 μ L of well solution (100 mM lithium sulfate, 100 mM sodium citrate, pH 5.5, 20% PEG 1000). S313A NSP2 mutant and Sh-NSP2 were crystallized similarly (0.16 M calcium acetate, 0.08 M sodium cacodylate, pH 6.5, 14.4% polyethylene glycol 8000, 20% glycerol). Crystals were transferred in a single step to the mother liquid for 1 min and then flash frozen in liquid nitrogen for diffraction data collection.

Structure Determination and Refinement. Data were collected at 100 K at the Advanced Light Source synchrotron beamline 5.0.1 and processed using HKL2000 (53) or IMOSFLM as implemented in the CCP4 suite (54). The molecular replacement (MR) was carried out by using the program PHASER (55) with the WT NSP2 structure (PDB ID code 1L9V) as a search model. Model building was performed using COOT (56). Iterative rounds of refinement, which included simulated annealing, translation/liberation/screw (TLS), and noncrystallographic symmetry constraints, and model building were carried out using PHENIX refinement (57). The data collection and refinement statistics are summarized in *SI Appendix, Table S5*. All structure figures were prepared using the University of California San Francisco Chimera program (58) and PyMOL (pymol.org). The formation of the disulfide bond between residues C8 and C85 in the crystal structure of WT SA11 Sh-NSP2 (PDB ID code 6CY9) was confirmed by computing a simulated annealing $F_o - F_c$ difference electron density map.

ACKNOWLEDGMENTS. This work was supported by National Institutes of Health (NIH) Grants R01 AI080656 (to M.K.E.), R37 AI 36040 (to B.V.V.P.), and Welch Foundation Grant Q1279 (to B.V.V.P.). This project was also supported by Advanced Technology Core Laboratories (Baylor College of Medicine), specifically the Integrated Microscopy Core at Baylor College of Medicine with funding from NIH (DK56338 and CA125123), Cancer Prevention & Research Institute of Texas (CPRI) (RP150578), the Dan L. Duncan Comprehensive Cancer Center, the John S. Dunn Gulf Coast Consortium for Chemical

Genomics; and the University of Texas Medical Branch (UTMB), Galveston Mass Spectrometry Facility with funding support from the University of Texas System Proteomics Network. The Berkeley Center for Structural Biology is supported in part by the NIH, National Institute of General Medical Sciences (P30 GM124169), and the Howard Hughes Medical Institute. The Advanced Light Source is supported by the Director, Office of Science, Office of Basic Energy Sciences, of the Department of Energy under Contract DE-AC02-05CH11231.

- Netherton C, Moffat K, Brooks E, Wileman T (2007) A guide to viral inclusions, membrane rearrangements, factories, and viroplasm produced during virus replication. *Adv Virus Res* 70:101–182.
- Dolnik O, Stevermann L, Kolesnikova L, Becker S (2015) Marburg virus inclusions: A virus-induced microcompartment and interface to multivesicular bodies and the late endosomal compartment. *Eur J Cell Biol* 94:323–331.
- Romero-Brey I, Bartschlag R (2014) Membranous replication factories induced by plus-strand RNA viruses. *Viruses* 6:2826–2857.
- Tate JE, Burton AH, Boschi-Pinto C, Parashar UD; World Health Organization–Coordinated Global Rotavirus Surveillance Network (2016) Global, regional, and national estimates of rotavirus mortality in children <5 years of age, 2000–2013. *Clin Infect Dis* 62(Suppl 2):S96–S105.
- Fabbretti E, Afrikanova I, Vascotto F, Burrone OR (1999) Two non-structural rotavirus proteins, NSP2 and NSP5, form viroplasm-like structures in vivo. *J Gen Virol* 80:333–339.
- Silvestri LS, Taraporewala ZF, Patton JT (2004) Rotavirus replication: Plus-sense templates for double-stranded RNA synthesis are made in viroplasm. *J Virol* 78:7763–7774.
- López T, Rojas M, Ayala-Bretón C, López S, Arias CF (2005) Reduced expression of the rotavirus NSP5 gene has a pleiotropic effect on virus replication. *J Gen Virol* 86:1609–1617.
- Vascotto F, Campagna M, Visintin M, Cattaneo A, Burrone OR (2004) Effects of intrabodies specific for rotavirus NSP5 during the virus replicative cycle. *J Gen Virol* 85:3285–3290.
- Campagna M, Eichwald C, Vascotto F, Burrone OR (2005) RNA interference of rotavirus segment 11 mRNA reveals the essential role of NSP5 in the virus replicative cycle. *J Gen Virol* 86:1481–1487.
- Eichwald C, Rodriguez JF, Burrone OR (2004) Characterization of rotavirus NSP2/NSP5 interactions and the dynamics of viroplasm formation. *J Gen Virol* 85:625–634.
- Eichwald C, Vascotto F, Fabbretti E, Burrone OR (2002) Rotavirus NSP5: Mapping phosphorylation sites and kinase activation and viroplasm localization domains. *J Virol* 76:3461–3470.
- Viskowska M, et al. (2014) Probing the sites of interactions of rotaviral proteins involved in replication. *J Virol* 88:12866–12881.
- Kattoura MD, Clapp LL, Patton JT (1992) The rotavirus nonstructural protein, NS35, possesses RNA-binding activity in vitro and in vivo. *Virology* 191:698–708.
- Vasquez-Del Carpio R, Gonzalez-Nilo FD, Riadi G, Taraporewala ZF, Patton JT (2006) Histidine triad-like motif of the rotavirus NSP2 octamer mediates both RTPase and NTPase activities. *J Mol Biol* 362:539–554.
- Kumar M, et al. (2007) Crystallographic and biochemical analysis of rotavirus NSP2 with nucleotides reveals a nucleoside diphosphate kinase-like activity. *J Virol* 81:12272–12284.
- Criglar JM, et al. (2014) A novel form of rotavirus NSP2 and phosphorylation-dependent NSP2-NSP5 interactions are associated with viroplasm assembly. *J Virol* 88:786–798.
- Hu L, et al. (2012) Crystallographic analysis of rotavirus NSP2-RNA complex reveals specific recognition of 5' GG sequence for RTPase activity. *J Virol* 86:10547–10557.
- Welch SK, Crawford SE, Estes MK (1989) Rotavirus SA11 genome segment 11 protein is a nonstructural phosphoprotein. *J Virol* 63:3974–3982.
- Poncet D, Lindenbaum P, L'Haridon R, Cohen J (1997) In vivo and in vitro phosphorylation of rotavirus NSP5 correlates with its localization in viroplasm. *J Virol* 71:34–41.
- Afrikanova I, Miozzo MC, Giambiagi S, Burrone O (1996) Phosphorylation generates different forms of rotavirus NSP5. *J Gen Virol* 77:2059–2065.
- Contin R, Arnoldi F, Campagna M, Burrone OR (2010) Rotavirus NSP5 orchestrates recruitment of viroplasmic proteins. *J Gen Virol* 91:1782–1793.
- Knippschild U, et al. (2014) The CK1 family: Contribution to cellular stress response and its role in carcinogenesis. *Front Oncol* 4:96.
- Eichwald C, Jacob G, Muszynski B, Allende JE, Burrone OR (2004) Uncoupling substrate and activation functions of rotavirus NSP5: Phosphorylation of Ser-67 by casein kinase 1 is essential for hyperphosphorylation. *Proc Natl Acad Sci USA* 101:16304–16309.
- Campagna M, et al. (2007) Impaired hyperphosphorylation of rotavirus NSP5 in cells depleted of casein kinase 1 α is associated with the formation of viroplasm with altered morphology and a moderate decrease in virus replication. *J Gen Virol* 88:2800–2810.
- Afrikanova I, Fabbretti E, Miozzo MC, Burrone OR (1998) Rotavirus NSP5 phosphorylation is up-regulated by interaction with NSP2. *J Gen Virol* 79:2679–2686.
- Taraporewala Z, Chen D, Patton JT (1999) Multimers formed by the rotavirus non-structural protein NSP2 bind to RNA and have nucleoside triphosphatase activity. *J Virol* 73:9934–9943.
- Shrestha A, Hamilton G, O'Neill E, Knapp S, Elkins JM (2012) Analysis of conditions affecting auto-phosphorylation of human kinases during expression in bacteria. *Protein Expr Purif* 81:136–143.
- Pulgar V, et al. (1999) Optimal sequences for non-phosphate-directed phosphorylation by protein kinase CK1 (casein kinase-1)—A re-evaluation. *Eur J Biochem* 260:520–526.
- Marin O, Meggio F, Sarno S, Andretta M, Pinna LA (1994) Phosphorylation of synthetic fragments of inhibitor-2 of protein phosphatase-1 by casein kinase-1 and -2. Evidence that phosphorylated residues are not strictly required for efficient targeting by casein kinase-1. *Eur J Biochem* 223:647–653.
- Jayaram H, Taraporewala Z, Patton JT, Prasad BV (2002) Rotavirus protein involved in genome replication and packaging exhibits a HIT-like fold. *Nature* 417:311–315.
- Gaunt ER, et al. (2013) Lipidome analysis of rotavirus-infected cells confirms the close interaction of lipid droplets with viroplasm. *J Gen Virol* 94:1576–1586.
- Cheung W, et al. (2010) Rotaviruses associate with cellular lipid droplet components to replicate in viroplasm, and compounds disrupting or blocking lipid droplets inhibit viroplasm formation and viral replication. *J Virol* 84:6782–6798.
- Flotow H, et al. (1990) Phosphate groups as substrate determinants for casein kinase I action. *J Biol Chem* 265:14264–14269.
- Prevost C, et al. (2018) Mechanism and determinants of amphipathic helix-containing protein targeting to lipid droplets. *Dev Cell* 44:73–86.e4.
- Nolen B, Taylor S, Ghosh G (2004) Regulation of protein kinases; controlling activity through activation segment conformation. *Mol Cell* 15:661–675.
- Beenstock J, Mooshayef N, Engelberg D (2016) How do protein kinases take a selfie (autophosphorylate)? *Trends Biochem Sci* 41:938–953.
- Jakubiec A, Jupin I (2007) Regulation of positive-strand RNA virus replication: The emerging role of phosphorylation. *Virus Res* 129:73–79.
- Keck F, Ataey P, Amaya M, Bailey C, Narayanan A (2015) Phosphorylation of single stranded RNA virus proteins and potential for novel therapeutic strategies. *Viruses* 7:5257–5273.
- Mondal A, Potts GK, Dawson AR, Coon JJ, Mehle A (2015) Phosphorylation at the homotypic interface regulates nucleoprotein oligomerization and assembly of the influenza virus replication machinery. *PLoS Pathog* 11:e1004826.
- Masaki T, et al. (2014) Involvement of hepatitis C virus NS5A hyperphosphorylation mediated by casein kinase I- α in infectious virus production. *J Virol* 88:7541–7555.
- Lee KY, Chen YH, Hsu SC, Yu MJ (2016) Phosphorylation of serine 235 of the hepatitis C virus non-structural protein NS5A by multiple kinases. *PLoS One* 11:e0166763.
- Eyre NS, et al. (2016) Phosphorylation of NS5A Serine-235 is essential to hepatitis C virus RNA replication and normal replication compartment formation. *Virology* 491:27–44.
- Bhattacharya D, Ansari IH, Striker R (2009) The flaviviral methyltransferase is a substrate of Casein Kinase 1. *Virus Res* 141:101–104.
- Bhattacharya D, et al. (2008) Phosphorylation of yellow fever virus NS5 alters methyltransferase activity. *Virology* 380:276–284.
- Dong H, et al. (2008) West Nile virus methyltransferase catalyzes two methylations of the viral RNA cap through a substrate-repositioning mechanism. *J Virol* 82:4295–4307.
- Kroschewski H, et al. (2008) Mutagenesis of the dengue virus type 2 NS5 methyltransferase domain. *J Biol Chem* 283:19410–19421.
- Keating JA, et al. (2013) West Nile virus methyltransferase domain interacts with protein kinase G. *Viral J* 10:242.
- Chattopadhyay S, et al. (2010) Computational identification of post-translational modification sites and functional families reveal possible moonlighting role of rotaviral proteins. *Bioinformatics* 4:448–451.
- Spencer KA, Dee M, Britton P, Hiscox JA (2008) Role of phosphorylation clusters in the biology of the coronavirus infectious bronchitis virus nucleocapsid protein. *Virology* 370:373–381.
- Kanai Y, et al. (2017) Entirely plasmid-based reverse genetics system for rotaviruses. *Proc Natl Acad Sci USA* 114:2349–2354.
- Keating JA, Striker R (2012) Phosphorylation events during viral infections provide potential therapeutic targets. *Rev Med Virol* 22:166–181.
- Crawford SE, Hyser JM, Utama B, Estes MK (2012) Autophagy hijacked through viroporin-activated calcium/calmodulin-dependent kinase kinase- β signaling is required for rotavirus replication. *Proc Natl Acad Sci USA* 109:E3405–E3413.
- Otwiniowski Z, Minor W (1997) Processing of X-ray diffraction data collected in oscillation mode. *Methods Enzymol* 276:307–326.
- Collaborative Computational Project, Number 4 (1994) The CCP4 suite: Programs for protein crystallography. *Acta Crystallogr D Biol Crystallogr* 50:760–763.
- McCoy AJ, et al. (2007) Phaser crystallographic software. *J Appl Crystallogr* 40:658–674.
- Emsley P, Lohkamp B, Scott WG, Cowtan K (2010) Features and development of Coot. *Acta Crystallogr D Biol Crystallogr* 66:486–501.
- Adams PD, et al. (2010) PHENIX: A comprehensive Python-based system for macromolecular structure solution. *Acta Crystallogr D Biol Crystallogr* 66:213–221.
- Pettersen EF, et al. (2004) UCSF Chimera—A visualization system for exploratory research and analysis. *J Comput Chem* 25:1605–1612.